DOI 10.1515/ama-2016-0010

APPLICATION OF A SPH COUPLED FEM METHOD FOR SIMULATION OF TRIMMING OF ALUMINUM AUTOBODY SHEET

Łukasz BOHDAL*

*Faculty of Mechanical Engineering, Koszalin University of Technology, Racławicka 15-17 str., 75-620 Koszalin, Poland

lukasz.bohdal@tu.koszalin.pl

received 5 April 2015, revised 23 February 2016, accepted 24 February2016

Abstract: In this paper, the applications of mesh-free SPH (Smoothed Particle Hydrodynamics) continuum method to the simulation and analysis of trimming process is presented. In dealing with shearing simulations for example of blanking, piercing or slitting, existing literatures apply finite element method (FEM) to analysis of this processes. Presented in this work approach and its application to trimming of aluminum autobody sheet allows for a complex analysis of physical phenomena occurring during the process without significant deterioration in the quality of the finite element mesh during large deformation. This allows for accurate representation of the loss of cohesion of the material under the influence of cutting tools. An analysis of state of stress, strain and fracture mechanisms of the material is presented. In experimental studies, an advanced vision-based technology based on digital image correlation (DIC) for monitoring the cutting process is used.

Key words: Trimming, Smoothed Particle Hydrodynamics, Digital Image Correlation

1. INTRODUCTION

The process of forming parts from sheet metal using shearing frequently includes blanking, piercing, slitting, and trimming operations. This operations realized with high speed, are a very complicated technological processes in which material undergoes plastic deformations. The main challenge when analyzing trimming is to obtain high quality products characterized optimum sheared edge condition, freedom from burrs and residual stresses. In the automotive industry for instance, burrs formed in the trimming process often scratch the surface of the formed parts in the downstream processes. In order to satisfy the existing standards of quality and to meet customer satisfaction requirements, stamped parts frequently need an additional deburring operation. Therefore, deburring adds significantly to the cost of a stamped part (Golovashchenko, 2006).

Knowledge of the trimming process is based mainly on experimental methods, which are often expensive and unable to be extrapolated to other cutting configurations. Trimming modelling is becoming an increasingly important tool in gaining understanding and improving this process. At the moment the trimming numerical models are based on Lagrangian or Arbitrary Lagrangian Eulerian (ALE) Finite Element Methods (FEM) (Golovashchenko, 2007; Hilditch and Hodgson, 2005b).

The operation of trimming has been studied with respect to sheared edge morphology (Golovashchenko, 2006; Li, 2000) shearing parameters optimization (Ilinichet al., 2011), residual stress analysis, or forming defects using FEM (Hilditch and Hodgson, 2005b; Golovashchenko, 2007). An analysis of the current literature suggests that these approaches imply difficulties. The difficulty in modeling this kind of process using FEM is that all the stages of the material behavior have to be represented: elastoplasticity, damage, crack initiation and propagation, and failure. Many of problems are resulted from the use of mesh, which should always ensure that the numerical compatibility condition is the same as the physical compatibility condition for a continuum. Hence, the use of grid/mesh can lead to various difficulties in dealing with problems with free surface, deformable boundary, moving interface, and extremely large deformation and crack propagation. Moreover, for problems with complicated geometry, the generation of a quality mesh has become a difficult, time-consuming and costly process.

Mentioned disadvantages of the finite element models can be eliminated using following mesh-free methods: smoothed particle hydrodynamics (SPH), element - free Galerkin method, amongst others (Heisel et al., 2013). SPH-method is used not only to describe the behavior of fluids and granular materials, but also for the modeling of large plastic deformation of solids, such as simulation of the orthogonal cutting processes (Bagci, 2011; Xi et al., 2014; Heisel et al., 2013) shoot peening (Jianming et al., 2011), or guillotining (Gąsiorek, 2013).

In this paper, the applications of mesh-free SPH methodology to the simulation and analysis of 3-D trimming process is presented. At the moment in current literature applications of mesh-free methods to modeling of trimming process is lacking. Developed model is used to analysis of residual stresses in workpiece during and after process under different conditions. Next, the model is validated with experimental research by using vision-based solutions. The proposed advanced vision-based technology is a modern tool which provide accurate measurement of sheet surface shape or deformation (displacement).

2. BASIS OF THE SPH METHOD

SPH is total Langrangian and is a truly mesh-free technique

DOI 10.1515/ama-2016-0010

initially developed by Gingold and Monaghan (1977) for the analysis and simulation of astrophysics problems. The idea of this method is to divide a continuum into discrete elements, called particles which are placed at some distance d from each other. This distance is called particle density d (Fig. 1).

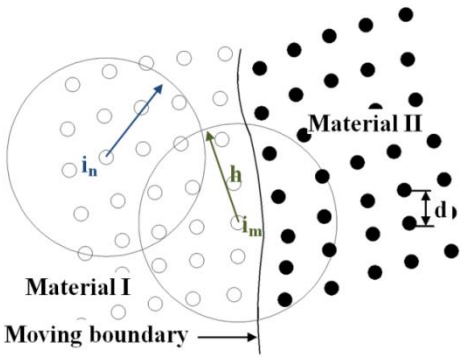

Fig. 1. Smoothing kernel in material volume and at the boundary

The smoothing of field variables is performed in the area with radius h, called the smoothing length, over which the variables are smoothed by a kernel function. This means that the value of a variable in any spatial point can be obtained by adding the relevant values of the variables within two smoothed circles. Sometimes relative to particle density smoothing length $\bar{h} = h/d$ is used. In contrast to mesh methods such as, e.g., the FEM, in which the mesh distorts in the case of large deformations, the SPH method can be used to model processes accompanied by large deformations. The SPH approximation of the searched function for continuum mechanics uses the following approaches. A function $f(x)$ is substituted by its approximation $A_f(x,h)$, characterising a body condition. For example, the velocities of a body's points in a particular area are approximated with the following expression:

$$A_f(x,h) = \int f(y) \cdot W(x,h)dy, \tag{1}$$

where: $W(x,h)$ is a smoothed kernel function (Heisel et al., 2013). The size of the smoothing kernel is defined by the function of Θ :

$$W(x,h) = \left(\frac{1}{h(x)^p}\right) \cdot \Theta(x), \tag{2}$$

where: p is the dimension of space (Das and Cleary, 2007).

The majority of the smoothing kernels used in the SPH method is represented as cubic B-spline, determining the selection of the function Θ as follows:

$$\Theta(x) = C \cdot \begin{cases} 1 - \frac{3}{2} \cdot x^2 + \frac{3}{4} \cdot x^3, & if |x| \le 1 \\ \frac{1}{4} \cdot (2-x)^3, & if\ 1 \le |x| \le 2 \\ 0 & if\ 2 \le |x| \end{cases} \tag{3}$$

where: C is the normalisation constant. Integration time step can be determined by following equation:

$$\Delta\tau = C_{\Delta\tau} \cdot min_i \left(\frac{h_i}{C_i + v_i}\right), \tag{4}$$

where: i is the particle number; $C_{\Delta\tau}$ is the timestep increase coefficient (in this work $C_{\Delta\tau} = 0.2$); v_i is the velocity of particle i. It is important to notice that coefficient $C_{\Delta\tau}$ directly influences the integration time step.

The smoothing length in LS-DYNA solver used in this work dynamically varies so that the number of neighbouring particles remains relatively constant. It is realized by recalculating the smoothing length in accordance with the average particle density:

$$h = h_0 \left(\frac{d_0}{d_i}\right)^{1/p}, \tag{5}$$

or by solving the continuity equation:

$$\frac{dh}{dt} = \frac{1}{d} \cdot \frac{h}{d} \cdot \frac{\partial d}{\partial t}, \tag{6}$$

where: d_0 and h_0 are the initial density and the initial smoothing length.

A quadratic approximation of the particle motion is mainly used for the SPH method. A motion of the particles can be described here with the following equation:

$$\frac{\partial v_i^\alpha}{\partial t} = \sum_{j=1}^{N} m_j \cdot \left(\frac{\sigma_i^{\alpha\beta}}{d_i^2} + \frac{\sigma_j^{\alpha\beta}}{d_j^2} + A_{ij}\right) \cdot \frac{\partial W_{ij}}{\partial x_i^\beta}, \tag{7}$$

where: j is particle number; N is the number of neighbouring particles; d_i and d_j are the densities of i and j particles respectively; A_{ij} are the specific external forces; $W_{ij} = W(x_i - x_j, h)$ is the smoothing kernel; $\mathrm{v_i^\alpha} = \frac{\mathrm{dx_i^\alpha}}{\mathrm{dt}}$ is the velocity of particle i; m_j is the mass of particle j; $\sigma_i^{\alpha\beta}, \sigma_j^{\alpha\beta}$, are the stress tensors of i and j particles respectively (Heisel et al., 2013).

3. CONSTITUTIVE MODEL FOR MATERIAL

In trimming models, accurate and reliable flow stress models are considered as highly necessary to represent workpiece materials' constitutive behavior, the constitutive material model reported by Johnson and Cook (1985) was employed in this study, it is often used for ductile materials in cases where strain rate vary over a large range and where adiabatic temperature increase due to plastic heating cause material softening. The model can be represented by Eq (8):

$$\sigma_Y = [A + B(\bar{\varepsilon}^p)^n][1 + Cln\dot{\varepsilon}^*][1 - (T^*)^m], \tag{8}$$

where: $A, B,$ and n are strain hardening constants; C is the strain rate hardening constant, σ_Y is the equivalent flow stress, $\bar{\varepsilon}^p$ is the equivalent plastic strain and m is the thermal softening constant that modifies the homologous temperature term, T^*. The homologous temperature is defined as, $T^* = \frac{T - T_r}{T_m - T_r}$, where T is the temperature of the material, T_r is a reference temperature (typically room temperature), and T_m is the melt temperature of the material. The term, $\dot{\varepsilon}^*$, is the normalized strain rate of the material or $\dot{\varepsilon}^* = \frac{\dot{\bar{\varepsilon}}^p}{\dot{\varepsilon}_0}$, where $\dot{\varepsilon}_0 = 1.0s^{-1}$.

Tab. 1. The Johnson-Cook constitutive model constants for AA6111-T4

$A\ [MPa]$	$B\ [MPa]$	C	n	m
324.1	113.8	0.002	1.34	0.42

The failure model must accurately predict the material equivalent plastic failure strain for various stress states, strain rates, and temperatures. The Johnson Cook failure model is:

$$\bar{\varepsilon}_f^p = \left[D_1 + D_2 e^{D_3 \sigma^*}\right][1 + D_4 ln\dot{\varepsilon}^*][1 + D_5 T^*], \tag{9}$$

DOI 10.1515/ama-2016-0010

where: D_1, D_2, D_3, D_4 and D_5 are material specific constants, $\bar{\varepsilon}_f^p$ is the equivalent plastic failure strain of the material and σ^* is the stress triaxiality factor defined as $\sigma^* = \frac{\sigma_m}{\bar{\sigma}}$, where σ_m is the average of the three principle stresses. Aluminum alloy AA6111-T4, which is often employed for exterior panels in the automotive industry, is used to simulate typical production conditions. For AA6111-T4: $D_1 = -0.77; D_2 = 1.45; D_3 = -0.47; D_4 = 0; D_5 = 1.6$.

4. COUPLED SPH+FEM MODEL

In the suggested approach to the modeling of the trimming process, a coupling of the FEM model and the model based on hydrodynamic particles (the SPH method) has been proposed. The one big disadvantage of meshless methods over the Lagrangian models is their computational demand. For that reason, in the trimming model, only an area in which there is a direct interaction between the upper knife and the sheet metal is modeled with SPH particles (Fig. 2). In the case of the SPH approach, the particles are tied to the Lagrangian portion of domain using tied types of the contact. The implementation of the SPH method in LS-DYNA allows for seamless transition between the two domains without resorting to the contact definitions. A three-dimensional model of trimming is built in LS - DYNA solver. Numerical calculations are performed for the 3D state of strain and 3D state of stress in this model.

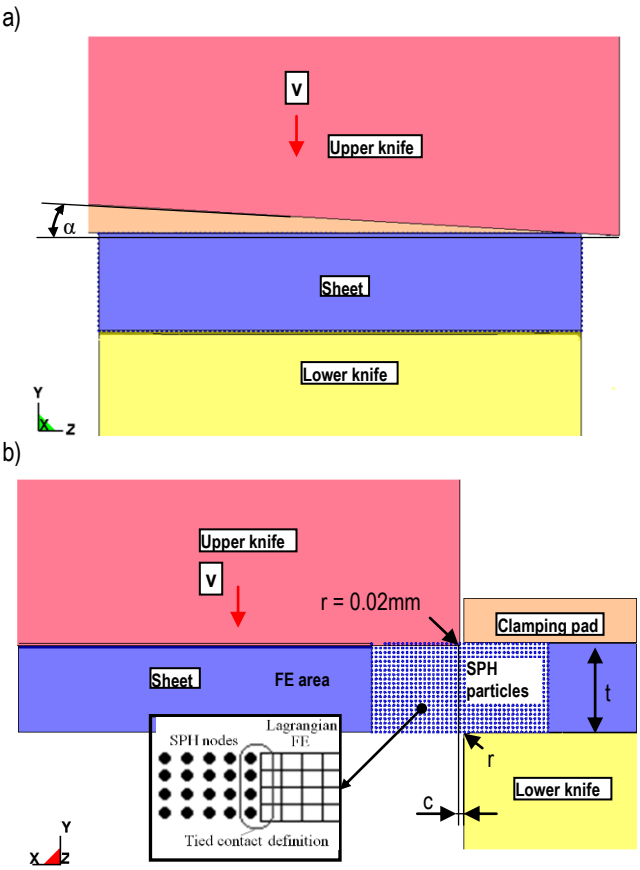

Fig. 2. FEM+SPH coupled model: a) side view; b) front view

Aluminum alloy with thickness of t = 1 mm is used as the material to be cut in the numerical and experimental studies. A velocity of $v = 100$ mm/s is applied to the upper knife in the y direction. The contact between ideally rigid tools and the deformable sheet metal is described using Coulomb's friction model, and constant coefficients of static friction $\mu_s = 0.08$ and kinetic friction $\mu_d = 0.009$ are accepted. A rake angle of upper knife is set about $\alpha = 3^\circ$ and clearance $c = 0.1$ mm.

5. RESULTS AND DISCUSSION

5.1. Analysis of trimming mechanism

Sample results of numerical and experimental investigations at various stages of the trimming process are shown in Figs. 3–5. At the beginning of the cutting process during the elastic-plastic phase the plasticised zone occurs only at the highest concentration of stresses, that is in direct contact with the cutting edges of tools. During the second phase the intensive plastic flow of the material in the surroundings of the cutting surface can be observed (Fig. 3a). A characteristic distortion of SPH particles in this areas can be seen. The highest stresses occurs near the cutting edges of the tools in this phase ($\sigma_{max} = 411$ MPa). Figure 3b shows the image from a high-speed camera i-SPEED TR in the same phase of process.

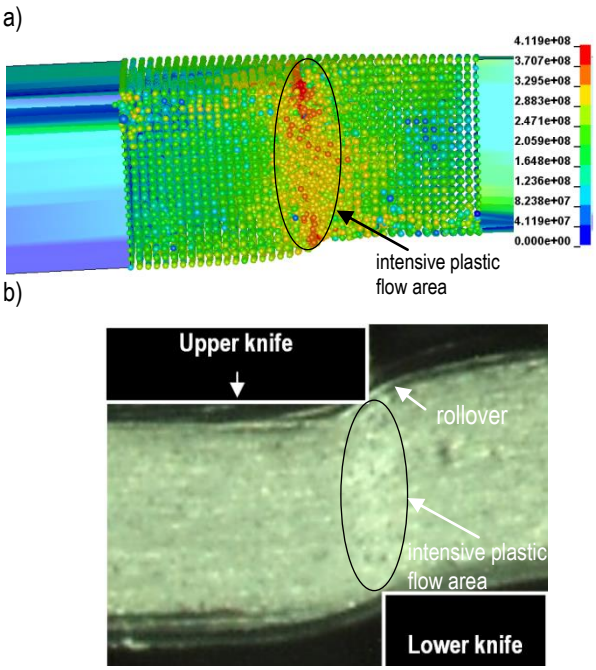

Fig. 3. Comparison of the numerical and experimental results for upper knife penetration w = 0.25 mm: a) FEM+SPH model (equivalent stress distribution [Pa]), b) recorded image from a high-speed camera

During the trimming process, a camera together with a computer record a set of consecutive images of the sample surface. To quantify the displacements of material, a digital image correlation technique (DIC) is used (Domski and Katzer, 2013). In two-dimensional digital image correlation, displacements are directly detected from digital images of the surface of an object (speci-

DOI 10.1515/ama-2016-0010

men) (Kozicki and Tejchman, 2007). Then, the images on the surface of the object, one before and another after deformation are recorded and saved in a computer as digital images. These images are compared to detect displacements by searching a characteristic features from one image to another. This features might be material texture, machining marks (for example an area of multiple pixel points), oxide deposits, finishing/polishing marks. Using this method it is possible to determine the areas of strong nonlinearities and deformation of material structure (Fig. 3b). The formation of rollover can be identified.

Both in numerical model and experimental investigations the plastic strain localization zones propagate much faster from the moving (upper knife) blade than from the bottom stationary blade (Fig 4c). The deformation zone is non-symmetric with respect to the top and bottom blades (Fig. 4). According to work (Li, 2000) this is not due to dynamic (or inertial) effects but rather to the shearing configuration of the experimental setup. It can be observed the large distortions of the SPH particles near the bottom edge of sheet just before burr formation (Fig. 4a). The mechanically affected zone in this area is extended along the x direction (Figs. 4a and b).

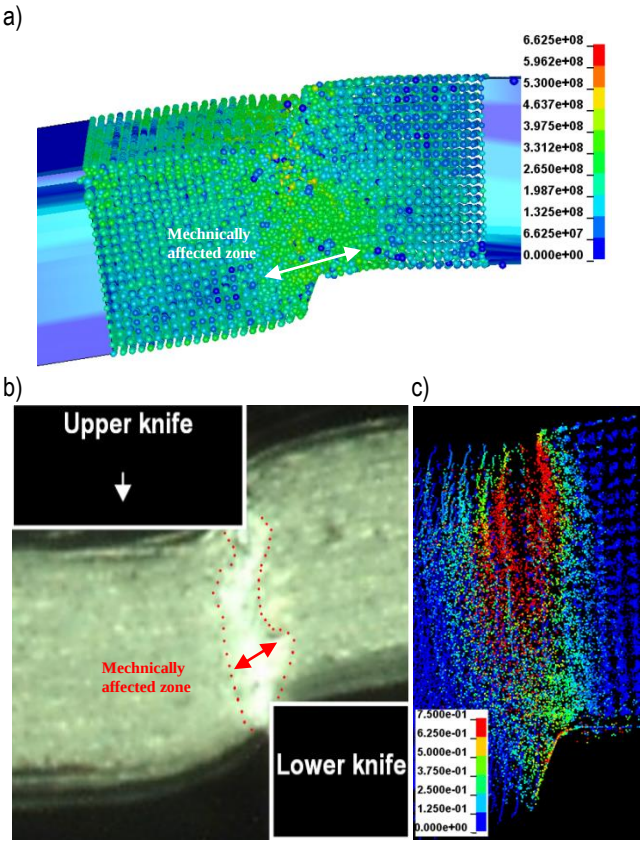

Fig. 4. Comparison of the numerical and experimental results for upper knife penetration w = 0.35 mm: a) FEM+SPH model (equivalent stress distribution), b) recorded image from a high-speed camera (deformation zone is extended on a whole sheet thickness and along x direction which is observed as an area with high light intensity), c) FEM+SPH model (equivalent strain distribution in contact zone)

Fig. 5 shows the equivalent stress and strain distribution during the cracking phase. Since the crack will initiate and propagate through the localization zone, the cut surface will be curved and the burr will form because the crack will not run to the bottom blade tip. This trend is evident in both the numerical model as well as experimental studies (Fig. 5). Results in the study by Golovashchenko (2006, 2007) and Hilditch (2005a), show that no burr formation occurs at clearances below 5% of the sheet thickness, attributed to the crack initiation in the sheet at the bottom blade tip. In mechanically affected zone a characteristic material flow along the crack path can be observed. To accurately measure the material flow on the surface of an object using DIC, a texture patterns need to be related to small group areas. Obtained results are in agreement with these experimental observations with approximately error margin about 5° in flowing angle measurement.

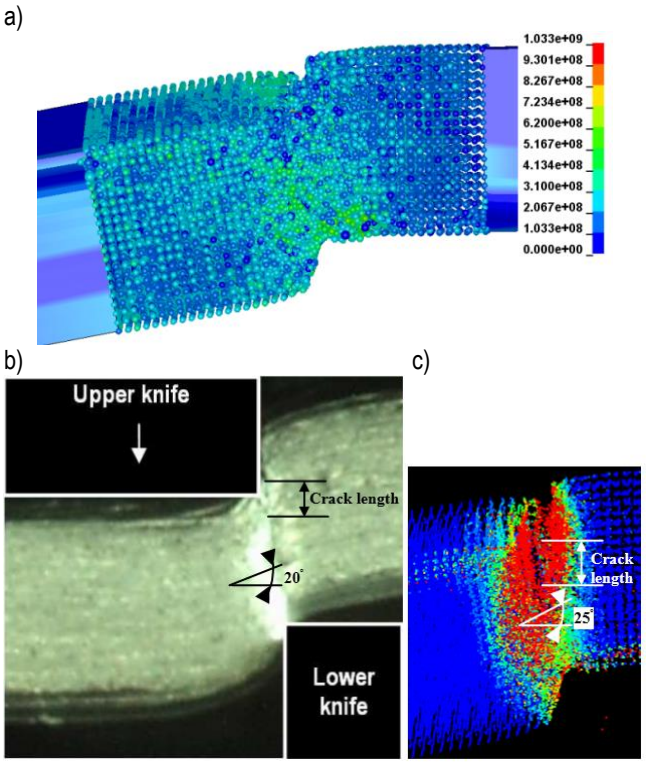

Fig. 5. Comparison of the numerical and experimental results for upper knife penetration w = 0,45 mm: a) FEM+SPH model (equivalent stress distribution), b) recorded image from a high-speed camera, c) FEM+SPH model (equivalent strain distribution in contact zone)

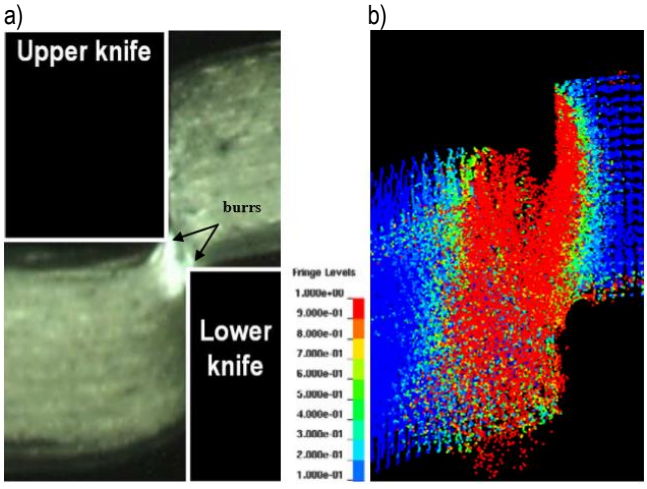

Fig. 6. Comparison of the numerical and experimental results at final separation: a) recorded image from a high-speed camera, b) FEM+SPH model (equivalent strain distribution in contact zone)

Łukasz Bohdal
DOI 10.1515/ama-2016-0010

5.2. Sheared edge quality

The quality of the sheared edge produced from the trimming of the sheet would depend upon the damage caused to the edge, the extent of the damage around the edge and burr height. The extend of the mechanically affected region can be quantified trough the equivalent plastic strain state. Strain measurements are made at three locations on the cut surface: without burr side, middle and burr side (Fig. 7).

An analysis of strain state shows that the maximum values of plastic strain occurs at the edge and then gradually decreases with increasing distance from the cut edge until it reaches a low constant value (Fig. 8). The measured results indicate that the maximum strain has reached a value of 1.5 at the middle of cut surface, and it exponentially decays away from the edge. The lowest values of strain occur in the upper part of the sample. The width of the deformed area is small and carry out approximately 0.1 mm.

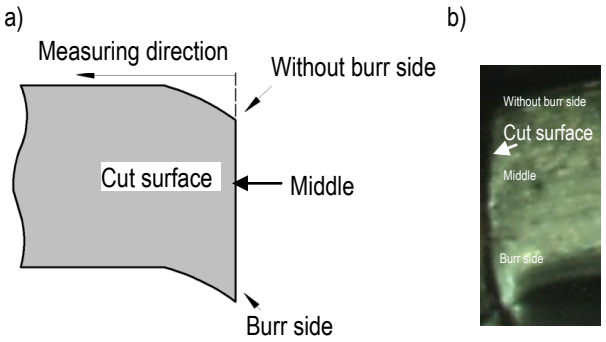

Fig. 7. Strain measurement areas at cut surface: a) schematic diagram, b) experimental profile

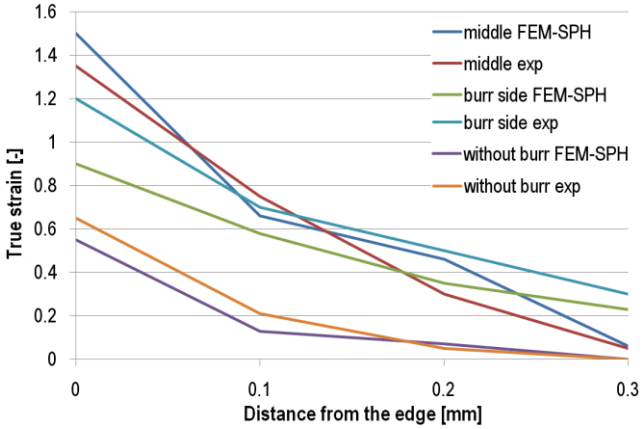

Fig. 8. Results of the true strain measured in sheared edge

Analysis of residual stress state in cut surface is presented on Fig 9. In the following, the von Misses equivalent stress is used to define and compare the residual stress state (Achouri et al., 2014) which is by definition is a complex three-dimensional stress state with interaction between the components of the stress tensor. In each analyzed cut surface area a high increase of stresses at a small tool penetration can be seen. In the initial phases of the cutting process the maximum stress values occur at the edge of cut surface and then decreases with increasing distance from the cut edge. During the workpiece forming large oscillations in stress values in unsteady state of process are observed. Stabilization of stresses occur after complete separation of the material and depends on distance from the edge. At any measured areas stress after stabilization did not exceed 200 MPa.

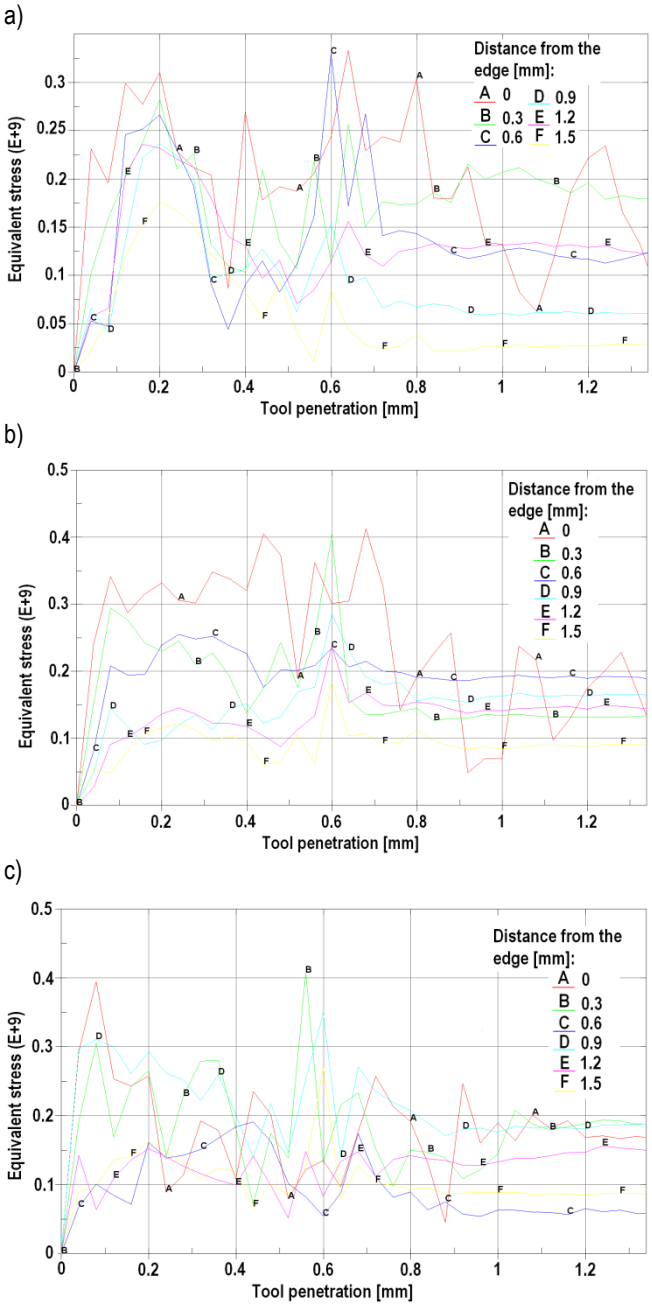

Fig. 9. Results of the equivalent stress measured in sheared edge during process [Pa]: a) without burr side, b) middle, c) burr side

Comparison of the characteristic features of cut surface obtained from numerical model and experiment shows good agreement in the depth angle and the burr height. Some differences occurs in the measurement of the rollover of the upper edge of workpiece (Fig. 10). Developed 3D FEM-SPH model of the trimming process allows for the observation of non-uniform burr at selected locations along the cutting line. From the results obtained it can be seen that the fracture process because less steady and progresses in a non-uniform manner in some locations along the

DOI 10.1515/ama-2016-0010

shearing line. The transition of the material fracture from the "shear mode" to the "shear and tear mode" is observed.

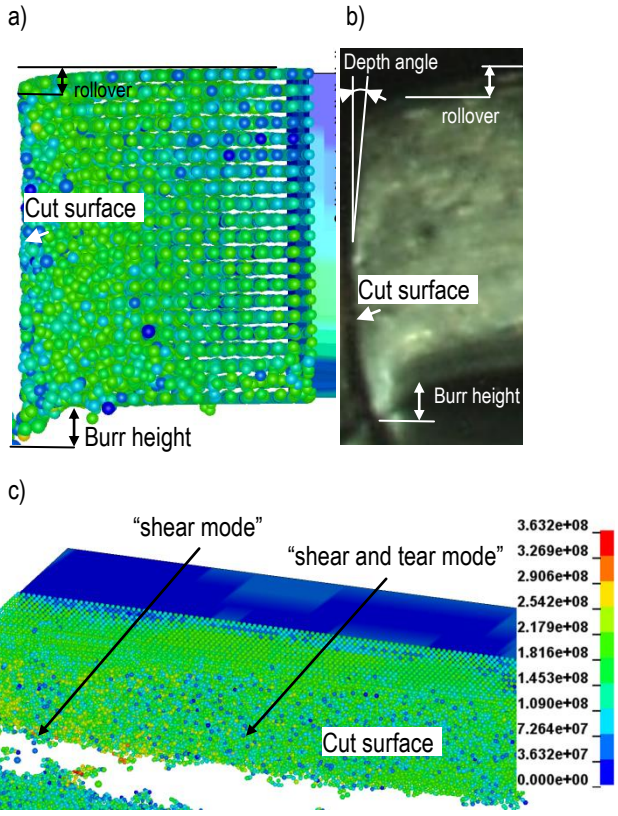

Fig. 10. Characteristic features of the sheared edge: a) FEM+SPH model (equivalent stress distribution – front view), b) experimental profile, c) FEM+SPH model (equivalent stress distribution - side view)

6. CONCLUSIONS

This paper presents a SPH coupled FEM method to simulate the trimming process. The application of SPH method is fairly new in metal forming simulations. Its features are not fully understood and the most effective means to exploit it are still being discovered. A hybrid approach that used the SPH formulation in the shearing zone with high material distortion and the Lagrangian formulation in the region away from the highly distorted zone is very robust and reliable. It reduces the simulation time needed to obtain the results. The FEM-SPH method is validated using the advanced vision based system and DIC method. Based on the experimental data, the model has been shown to be able to provide adequate estimation of the deformation state of material and might be used for process control as well as optimizing the trimming parameters. The good agreement between simulation results and the experimental data have confirmed the correctness and credibility of the model. Additionally, next paper will be focused on examination and analysis of influence of process technological parameters for example: the clearance, tool geometry, cutting velocity on residual stresses and quality of cut surface using the SPH method.

REFERENCES

1. **Achouri M., Gildemyn E., Germain G., Dal Santo P., Potiron A.** (2014), Influence of the edge rounding process on the behavior of blanked parts: numerical predictions with experimental correlation, *International Journal of Advanced Manufacturing Technology*, 71, 1019-1032.
2. **Bagci E.** (2011), 3-D numerical analysis of orthogonal cuttingprocess via mesh-free method, *International Journal of Physical Sciences*, 6, 1267-1282.
3. **Das R., Cleary PW.** (2007), Modeling plastic deformation andthermal response in welding using smoothed particle hydrodynamics,*16th Australasian fluid mechanics conference*, 2–7 December 2007.
4. **Domski J., Katzer J.** (2013), Load-deflection characteristic of fibre concrete based on waste ceramic aggregate, *Annual Set The Environment Protection* 15, 213-230.
5. **Gąsiorek D.** (2013), The application of the smoothed particle hydrodynamics (SPH) method and the experimental verification of cutting of sheet metal bundles using a guillotine, *Journal of Theoretical and Applied Mechanics,* 51 (4), 1053-1065.
6. **Gingold RA., Monaghan JJ.** (1977),Smooth particle hydrodynamics: theory and application to non-spherical stars, *Monthly Notices of the Royal Astronomical Society*, 181, 375-389.
7. **Golovashchenko S.F.** (2006), A study on trimming of aluminum autobody sheet and development of a new robust process eliminating burrs and slivers, *International Journal of Mechanical Sciences*, 48, 1384-1400.
8. **Golovashchenko S.F.** (2007), Analysis of Trimming of Aluminum Closure Panels, *JMEPEG* ,16, 213-219.
9. **Heisel U., Zaloga W., Krivoruchko D., Storchak M., Goloborodko L.** (2013), Modelling of orthogonal cutting processes with the methodof smoothed particle hydrodynamics, *Production Engineering Research and Development*, 7, 639-645.
10. **Hilditch T.B., Hodgson P.D.** (2005a), Development of the sheared edge in the trimming of steel and light metal sheet, Part 1 - Experimental observations, *Journal of Materials Processing Technology*, 169, 184-191.
11. **Hilditch T.B., Hodgson P.D.** (2005b), Development of the sheared edge in the trimming of steel and light metal sheet, Part 2 – Mechanisms and modeling,*Journal of Materials Processing Technology*, 169, 192-198.
12. **Ilinich A.M., Golovashchenko S.F., Smith L.M.** (2011), Material anisotropy and trimming method effects on total elongation in DP500 sheet steel, *Journal of Materials Processing Technology*, 211, 441-449.
13. **Jianming W., Feihong L., Feng Y., Gang Z.** (2011), Shot peening simulation based on SPH method, *International Journal of Advanced Manufacturing Technology*, 56, 571-578.
14. **Johnson G.R., Cook W.H.** (1985), Fracture characteristics of three metals subjected to various strains, strain rates, temperatures and pressures, *Engineering Fracture Mechanics,* 21(1), 31-48.
15. **Kozicki J., Tejchman J.** (2007), Experimental investigations of strain localization in concrete using digital image correlation (DIC) technique, *Archives of Hydro-Engineering and Environmental Mechanics,* 54(1), 3-24.
16. **Li M.** (2000), Micromechanisms of deformation and fracture in shearing aluminum alloy sheet, *International Journal of Mechanical Sciences*, 42, 907-923.
17. **Xi Y., Bermingham M., Wang G., Dargusch M.** (2014), SPH/FE modeling of cutting force and chip formation during thermally assisted machining of Ti6Al4V alloy, *Computational Materials Science*, 84, 188-197.